Electrochemistry and Spectroelectrochemistry of Chloro(phthalocyaninato)Rhodium(III) Species in Solution Phase

A. B. P. Lever,* Yuhong Tse, V. Manivannan, Penny Seymour, Vladimir V. Strelets, and Lalchan S. Persaud

Department of Chemistry, York University, North York (Toronto), Canada M3J 1P3

Received May 16, 1995[⊗]

The electrochemistry and spectroelectrochemistry of mononuclear chloro(phthalocyaninato)rhodium(III), $ClRh^{III}$-Pc, has been studied in the solution phase, at ambient and low temperature. Reduction leads to a rhodium(II) species, $ClRh^{II}Pc$ which is stable at low temperature, with reversible electrochemistry, but at ambient temperature dimerizes generating a rhodium−rhodium-bonded dinuclear species. This dinuclear species is oxidized at a much more positive potential than the mononuclear species. The complex electrochemical behavior of these species is shown to be due to the presence of three different dinuclear Rh^{II} species with zero, one, or two axially bound chloride ions whose detailed electrochemical properties are explored. Reduction of the dinuclear $Rh^{II}Pc$ species leads to a reversibly generated anion radical species.

Introduction

The electrochemistry of metallophthalocyanine species is very rich with many redox processes which may be localized on the metal or ligand;[1] such behavior is responsible for the considerable interest being shown in metallophthalocyanines as redox active chemical sensors.[2−10] We have previously noted that $Rh^{III}Pc$ species adsorbed on a graphite surface, form dinuclear derivatives when reduced to the $Rh^{II}Pc$ level.[11] Recently Nyokong[12a] has confirmed the formation of a dinuclear species when various $Rh^{III}Pc$ species are reduced to the $Rh^{II}Pc$ level in solution. Nyokong reports electrochemical and spectroscopic data for $(L)(L')Rh^{III}Pc(2-)$ species where L = Cl and L′ = Py or DMSO, and where L = L′ = CN (Py = pyridine, DMSO = dimethyl sulfoxide), in various, mostly coordinating solvents.

Liu[12b] has also briefly reported on the voltammetry of the $L_2Rh^{III}Pc$ species (L = H_2O, dimethylformamide (DMF)) proposing reduction to a $Rh^{II}Pc$ species but without recognizing that it forms a dinuclear species. Liu also reports electronic spectroscopic data for $Rh^{III}Pc(1-)$, the so-called $Rh^{II}Pc(2-)$, and what was in fact a $Rh^{II}Pc(3-)$ dinuclear species although it was not identified as such.

We has been investigating the electrochemical behavior of $ClRh^{III}Pc(2-)$ (**1,Cl**) and $ClRh^{III}TNPc(2-)$, (**TN,1,Cl**), in relation to our earlier surface chemistry study.[11] Our data add very considerable detail to these brief earlier reports.[12] More detailed cyclic voltammetric data, low temperature data, and cyclic voltammetric data for the bulk phase dinuclear species, absent from the previous analyses,[12] are presented here. We also disagree with certain of the conclusions of Nyokong[12a] and of Liu.[12b] Further, the electrochemical properties of these rhodium phthalocyanine systems[13−27] differ in detail from those of the corresponding rhodium porphyrins, as described by Kadish and co-workers.[28−31]

The key to understanding the very complex electrochemical behavior of chlororhodium phthalocyanine is the recognition that the mononuclear $Rh^{III}Pc$ species dimerizes when reduced to $Rh^{II}Pc$, at the process labeled **D** herein, that this dinuclear

[⊗] Abstract published in *Advance ACS Abstracts,* January 1, 1996.

(1) Lever, A. B. P.; Milaeva, E. R.; Speier, G. In *Phthalocyanines, Properties and Applications*; Leznoff, C. C., Lever, A. B. P., Eds.; VCH: New York, Vol. 3, 1993; p 1.
(2) Tse, Y. H.; Janda, P.; Lever, A. B. P. *Anal. Chem.* **1994**, *66*, 384.
(3) Tse, Y. H.; Janda, P.; Lam, H.; Lever, A. B. P. *Anal. Chem.* **1995**, *67*, 981.
(4) Inagaki, N.; Tasaka, S.; Ikeda, Y. *J. Appl. Polym. Sci.* **1995**, *55*, 1451. Mizutani, F.; Yabuki, S.; Iijima, S. *Anal. Chem. Acta* **1995**, *300*, 59. Jiang, D. P.; Lu, A. D.; Li, Y. J.; Pang, X. M.; Hua, Y. L. *Thin Solid Films* **1991**, *199*, 173.
(5) Dogo, S.; Germain, J. P.; Maleysson, C.; Pauly, A. *Thin Solid Films*, **1992**, *219*, 244.
(6) Sadaoka, Y.; Matsuguchi, M.; Sakai, Y.; Mori, Y. *J. Mater. Sci.* **1992**, *27*, 5215.
(7) Sun, Z. S.; Tachikawa, H. *Anal. Chem.* **1992**, *64*, 1112.
(8) Vukusic, P. S.; Sambles, J. R. *Thin Solid Films* **1992**, *221*, 311.
(9) Wring, S. A.; Hart, J. P. *Analyst* **1992**, *117*, 1215.
(10) Barancok, D.; Cirak, J.; Tomcik, P.; Brynda, E.; Nespurek, S. *Phys. Status Solidi A* **1993**, *138*, 191. Collins, G. E.; Armstrong, N. R.; Pankow, J. W.; Oden, C.; Brina, R.; Arbour, C.; Dodelet, J. P. *J. Vac. Sci. Technol. A* **1993**, *11*, 1383. Gilmartin, M. A. T.; Hart, J. P. *Analyst* **1994**, *119*, 833. Gu, C. Z.; Sun, L. Y.; Zhang, T.; Li, T. J.; Hirata, M. *Thin Solid Films* **1994**, *244*, 909.
(11) Tse, Y. H.; Seymour, P.; Kobayashi, N.; Lam, H.; Leznoff, C. C.; Lever, A. B. P. *Inorg. Chem.* **1991**, *31*, 4453.
(12) (a) Nyokong, T. *J. Chem. Soc., Dalton Trans.* **1994**, 1359. (b) Liu, W. *Wuji Huaxue Xuebao*, **1993**, *9*, 166.
(13) Hanack, H.; Munz, X. *Synth. Met.* **1985**, *10*, 357.
(14) Munx, X.; Hanack, M. *Chem. Ber.* **1988**, *121*, 239.
(15) Muralidharan, S.; Ferraudi, G.; Schmatz, K. *Inorg. Chem.* **1982**, *21*, 2961.
(16) Muralidharan, S.; Ferraudi, G. *J. Phys. Chem.* **1983**, *87*, 4877.
(17) Boucher, L. J. In *Coordination Chemistry of Macrocyclic Compounds*; Plenum: New York, 1979; p 461.
(18) Muenz, X.; Hanack, M. *Chem. Ber.* **1988**, *121*, 235.
(19) Sievertsen, S.; Ostendorp, G.; Homborg, H. *Z. Anorg. Allg. Chem.* **1994**, *620*, 290.
(20) Ferraudi, G.; Muralidharan, S. *Inorg. Chem.* **1983**, *22*, 1369.
(21) Van Vlierberge, B.; Ferraudi, G. *Inorg. Chem.* **1987**, *26*, 337.
(22) Ferraudi, G.; Oishi, S.; Muraldiharan, S. *J. Phys. Chem.* **1984**, *88*, 5261−4.
(23) Berezin, B. D. *Dokl. Acad. Nauk SSR* **1963**, *150*, 1039; Engl. Trans. p. 478.
(24) Hanack, M. *Isr. J. Chem.* **1985**, *25*, 205.
(25) Menzel, E. R.; Rieckhoff, K. E.; Voigt, E. M. *J. Chem. Phys.* **1973**, *58*, 5726−34.
(26) Schmatz, K.; Muralidharan, S.; Madden, K.; Fessenden, R.; Ferraudi, G. *Inorg. Chim. Acta* **1982**, *64*, L23.
(27) Chen, M. J.; Rathke, J. W. *Organometallics* **1994**, *13*, 4875. Chen, M. J.; Rathke, J. W. *J. Chem. Soc., Chem. Commun.* **1992**, 308.
(28) Anderson, J. E.; Yao, C-L.; Kadish, K. M. *Inorg. Chem.* **1986**, *25*, 3224.
(29) (a) Kadish, K. M.; Yao, C-L.; Anderson, J. E.; Cocolios, P. *Inorg. Chem.* **1985**, *24*, 4515. (b) Kadish, K. M.; Anderson, J. E.; Yao, C-L.; Guilard, R. *Inorg. Chem.* **1986**, *25*, 1277.
(30) Kadish, K. M.; Hu, Y.; Boschi, T.; Tagliatesta, P. *Inorg. Chem.* **1993**, *32*, 2996.

0020-1669/96/1335-0725$12.00/0

species is oxidized at a much more positive potential than mononuclear $Rh^{II}Pc$, at processes labeled **B**, **B′**, and **C** herein, and that there are in fact three different dinuclear species depending upon the extent of axial ligation by chloride ion.

Experimental Section

Materials. Tetrabutylammonium hexafluorophosphate ((TBA)PF_6; Aldrich) and tetraethylammonium chloride ((TEA)Cl; Aldrich) were recrystallized from absolute ethanol and dried in a vacuum oven at 120 °C for 24 hours. Tetrabutylammonium perchlorate (TBAP; Kodak) was recrystallized from absolute ethanol and dried in a vacuum oven at 50 °C for 2 days. 1,2-Dichlorobenzene (DCB, Aldrich) and *N*,*N*-Dimethylformamide (DMF; Aldrich) were used as supplied. Argon gas (Linde) was purified by passage through heated copper filings for electrochemical measurements.

Methods. Cyclic voltammetric measurements were performed with a Princeton Applied Research (PAR) Model 173 potentiostat or a PARC model polarographic analyzer coupled to a PARC Model 175 universal programmer, PARC Model 174A polarographic analyzer, or a Pine Instrument RDE-3 potentiostat. For the fast scan rate study ($v \geq 200$ mV/s), all electrochemical data were collected using a Model CS-900-UPG Computer Controlled Electroanalysis System (Cypress System, Inc., software version 5.0).

A conventional three electrode cell was used in electrochemical experiments. A platinum (Pt) disk described by the cross-sectional area of 0.196 mm^2 or a Pt disk with the diameter of 25 μm, sealed in glass, were used as the working electrode, a Pt wire as the counter electrode, and a AgCl/Ag or Ag wire as the quasi-reference electrode. Potentials were referenced internally to the ferrocenium/ferrocene (Fc^+/Fc) couple. Electronic spectra were recorded with a Guided Wave Inc. Model 100-20 optical waveguide spectrum analyzer or a Hitachi Perkin-Elmer Model 340 microprocessor spectrometer or a Cary Model 2400 spectrometer. FTIR spectra were obtained as Nujol mulls using a Nicolet 20 SX instrument.

Syntheses. Preparation, purification and characterization of chloro-(phthalocyaninato)rhodium(III) (**1,Cl**) ($ClRh^{III}Pc(2-)$) and chloro-(tetraneopentoxyphthalocyaninato)rhodium(III) (**TN,1,Cl**) ($ClRh^{III}$-$TNPc(2-)$) have been previously described.[11,14,17,18,32]

Results

(1) Cyclic Voltammetry (CV). The cyclic voltammetric behavior of rhodium(III) phthalocyanine is strongly dependent on solvent, supporting electrolyte and temperature. In the following sections we discuss the CV data obtained under specified conditions and show that its elucidation follows from controlled potential electrolysis and further CV and spectroelectrochemical analysis of the resulting bulk solutions. Two different species are investigated, chlororhodium(III) phthalocyanine (**1,Cl**) and the bulkier chlororhodium tetraneopentoxyphthalocyanine (**TN,1,Cl**); not all experiments were carried out with both species. Here and henceforth, the **Cl** refers to a chloride bound axially to the rhodium atom; the absence of this indicator refers to the general species without defining the axial ligand.

(1.1) Room temperature. (1.1.1) $ClRh^{III}Pc(2-)$, (1,Cl). TBAP or (TBA)PF_6 as Supporting Electrolyte (Figures 1 and 2). Scanning from +1.0 to −1.0 V in DMF or DCB at room temperature, species **1,Cl** showed a well defined redox couple,[33]

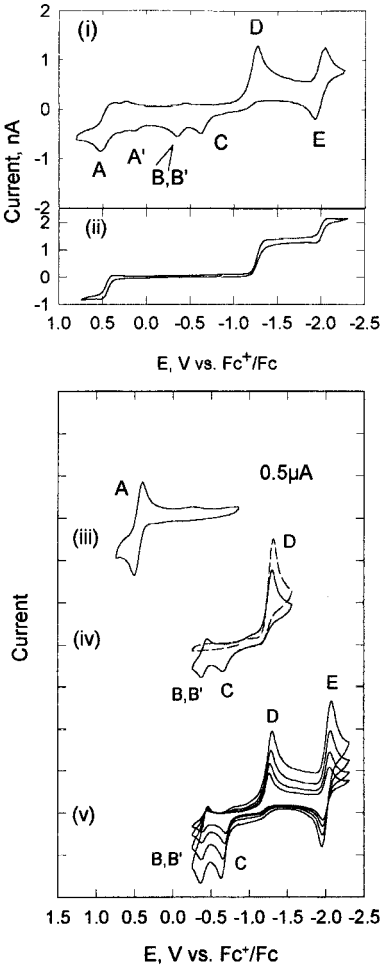

Figure 1. Cyclic voltammograms for species (**1,Cl**) in DCB (0.15 M TBAP, Pt working electrode): (i) scan rate 100 mV/s; (ii) cyclic voltammetry at a microelectrode, scan rate 20 mV/s; (iii) scan rate 100 mV/s; (iv) scan rate 100 mV/s, initial positive going scan from about −0.8 V (dot line) and steady scan (solid line); (v) steady state data, scan rates 25, 50, 100, 200, and 500 mV/s. Individual current divisions are 0.5 μA apart. In subsequent figures, individual current divisions are as indicated. Note: Figure 1(i) current divisions are 1 μA apart.

A, (Figure 1)(iii)) at about 0.5 V vs Fc^+/Fc, varying slightly with solvent. In this case $i_p \propto v^{1/2}$ (v = scan rate) and $i_a = i_c$, characteristic of a reversible electrode process. Couple **A** has been assigned as the oxidation of the Pc ring to the cation radical[1,12,32] $[ClRh^{III}Pc(1-)]^+$ (see spectroelectrochemical data discussed below). Data for all electrochemical experiments are summarized in Table 1.

The reduction of species **1,Cl** in DMF or DCB, at room temperature, is characterized by an irreversible peak **D** at about −1.2 V followed by a reversible couple **E** at about −1.9 V (Figures 1 and 2; Table 1). In addition to the observation of wave **D** and couple **E**, an ill-defined couple **B**, and an irreversible peak **C** (Figures 1 and 2) were observed in the potential range of −0.2 to −0.6 V *after* scanning negative of wave **D** (Figure 1(iv,v)); couples **B** and **C** therefore originate from a product generated negative of **D**, in fact the dinuclear $Rh^{II}Pc(2-)$ species.[11,12,27] (see Scheme 1). The anodic current for couple **B** was always larger than the cathodic current (with bulk species **1,Cl**), and we demonstrate below that there are two overlapping processes in this region, one giving rise to a

(31) Yao, C. L.; Anderson, J. E.; Kadish, K. M. *Inorg. Chem.* **1987**, *26*, 2725. Liu, Y. H.; Anderson, J. E.; Kadish, K. M. *Inorg. Chem.* **1988**, *27*, 2320. Anderson, J. E.; Liu, Y. H.; Kadish, K. M. *Inorg. Chem.* **1987**, *26*, 4174. Kadish, K. M.; Koh, W.; Tagliatesta, P.; Sazou, D.; Paolesse, R.; Licoccia, S.; Boschi, T. *Inorg. Chem.* **1992**, *31*, 2305. Anderson, J. E.; Yao, C. L.; Kadish, K. M. *Inorg. Chem.* **1986**, *25*, 718.

(32) The standard phthalocyanine has two negative charges and is written Pc(2−); thus the first ring oxidized species is written Pc(1−) and the first ring reduced species as Pc(3−). See: Myers, J. F.; Rayner Canham, G. W.; Lever, A. B. P. *Inorg. Chem.* **1975**, *14*, 461.

(33) Couples are identified generally by capital bold letters, e.g. **D**. When necessary, the anodic and cathodic current components are identified as $\mathbf{D_{an}}$ and $\mathbf{D_{cat}}$.

Scheme 1

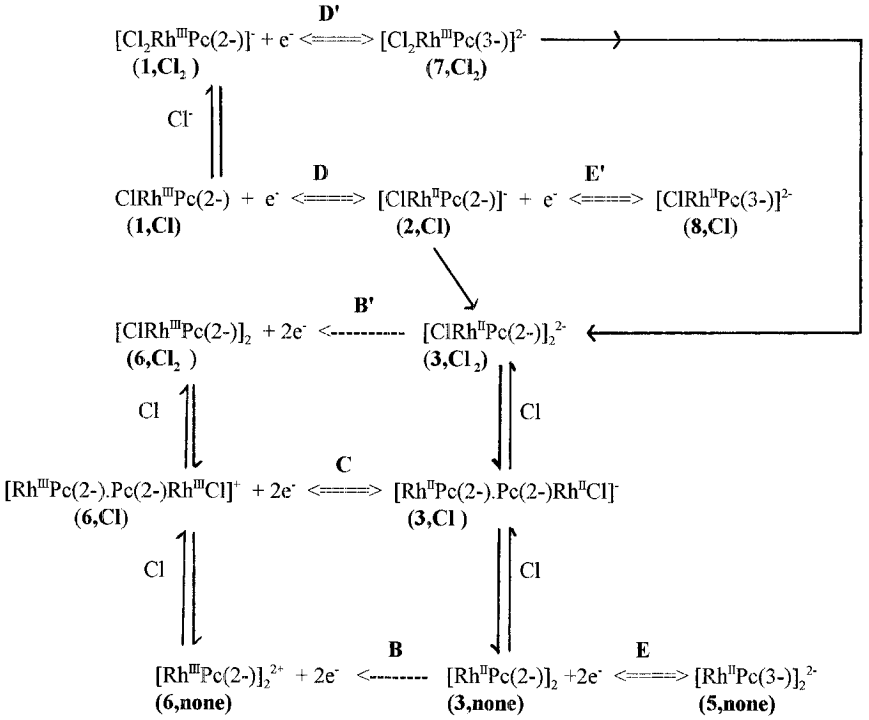

Table 1. Half-Wave Potentials (V vs Fc^+/Fc) of species (**1,Cl**) and (**TN,1**)[a,b]

ClRhPc	TBAP/ DMF	TBAP/ DCB	(TEA)Cl/ DMF	$(TBA)PF_6$/ DMF
A	0.57 (80)	0.47 (110)		0.54 (90)
B	−0.24 (65)	−0.39 (65)		−0.27 (55)
C[c]	−0.50	−0.61	−0.18	−0.51
D[c]	−1.09	−1.27	−1.13	−1.10
D′[c]			−1.29	
E	−1.87 (80)	−1.99 (110)	−1.86 (70)	−1.87 (80)

ClRhTNPc	TBAP/ DMF	(TEA)Cl/ DMF
A	0.30(80)	
B	−0.37	−0.34
C[c]	−0.50	
D[d]	−1.44 (80)	
D′		−1.53 (125)
E	−1.97 (80)	−1.95 (105)

[a] Half-wave potential was determined from the average of cathodic and anodic peak positions at scan rate = 100 mV/s; peak to peak separation is given in parentheses. [b] All solvents contained 0.15 M supporting electrolyte. [c] Irreversible. [d] Reversible at fast scan (see Figure 5).

electrochemically reversible process, which is labeled **B**, and one an irreversible process, showing only an anodic wing, labeled **B′**.

If after observing **B, B′,** and **C**, the scan is returned negatively but switched positive of **D** and cycled several times, wave **C** disappears after about six cycles (at 100 mV/s, in DMF) while wave **B,B′** declines in current becoming more reversible in appearance ($\mathbf{B_{an}} = \mathbf{B_{cat}}$) before eventually declining to zero. Note also that a steady state microelectrode scan shows waves **A**, **D**, and **E** but not **B, B′,** and **C** (Figure 1(ii)). With a slow scan rate (20 mV/s), the steady state currents, at the microelectrode, for processes **A, D,** and **E** were all approximately the same. Thus waves **B, B′,** and **C** arise from oxidation of the dinuclear species formed at **D**, on the surface of the electrode, and are therefore absent from the steady state microelectrode experiment. Scanning within the range 0 to −1.5 V (switching positive of wave **E**), the ratio of current intensity of **C**/**B** decreases with increasing scan rate. In such a scan rate study, the potential of wave **C** shifts positively with increasing scan rate, as its current diminishes. Wave **B** shows a small cathodic component when switched just positive of **B** (Figure 1(iv,v)), but if the cyclic is swept beyond **A** then the cathodic wave for **B** is absent, or very weak (depending on scan rate) (Figure 1(i)) when returning to the negative region.

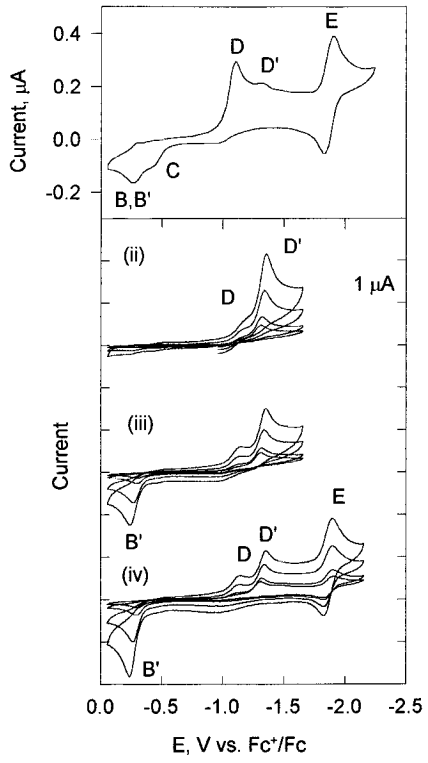

Figure 2. Cyclic voltammogram of $ClRh^{III}Pc(2-)$, (**1,Cl**) in DMF (0.15 M TBAP + 5.25×10^{-3} M (TEA)Cl) at a Pt electrode, steady state, scan rate 100 mV/s. Cyclic voltammograms for species (**1,Cl**) in DMF (0.15 M TEACl, Pt working electrode): (ii) initial scan, positive going from −1.0 V, scan rate 25, 50, 200, 500 mV/s; (iii,iv) steady state, scan rate: 25, 50, 200, and 500 mV/s.

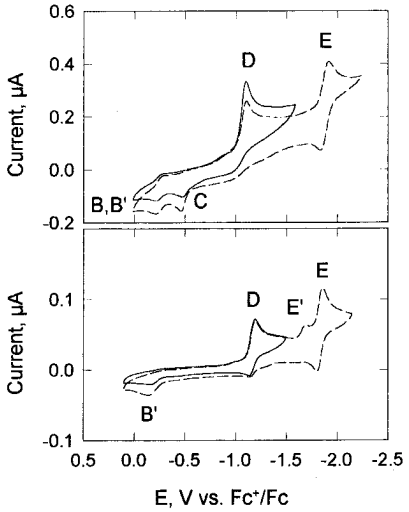

Figure 3. Cyclic voltammograms for species (**1,Cl**) in DMF (0.15 M TBAP, Pt working electrode): (i) scan rate 100 mV/s, room temperature; (ii) scan rate 100 mV/s, −72 °C. Steady state.

The peak position of **D** shifts by about −20 mV per decade with increasing scan rate and −20 mV/log[**1,Cl**] with decreasing concentration of species **1,Cl** consistent with dimerization. However, the $E_{1/2}$ of couple **E** was independent of the scan rate and concentration of species **1**. If a voltammogram containing waves **B, B′,** and **C** is scanned positively, then a weak shoulder is seen, labeled **A′,** just negative of **A** (Figure 1(i)). This is absent from voltammograms which do not exhibit **B, B′,** and **C** and is therefore a process originating through oxidation of a species involved in couple **B**, **B′,** or **C**.

(1.1.2) In the Presence of (TEA)Cl. The species **1,Cl** contains a chloride anion which may possibly be released into solution when the species is reduced. The cyclic voltammetric behavior was therefore investigated in the presence of additional chloride ion, as supporting electrolyte, in the form of tetraethylammonium chloride ((TEA)Cl). As demonstrated below (section 3 of the Results) the addition of chloride ion generates a new dichloro species, labeled **1,Cl$_2$** in equilibrium with **1,Cl**. When (TEA)Cl is the supporting electrolyte (Figure 2, Figure S1) the detailed behavior depends upon its concentration. With low (TEA)Cl concentration, (5.25×10^{-3} M) wave **D** is seen and a new wave **D′** is revealed, due to reduction of **1,Cl$_2$**, at about 200 mV negative of wave **D** (Figure 2(i)). Wave **E** is observed at its usual potential. After the species is cycled beyond **D′** or **E**, the cathodic component of wave **B** is almost lost (i.e. the process is mainly **B′**) and wave **C** is weakly observable (Figure 2(i)). As the (TEA)Cl concentration is increased (see Figure S1 for intermediate (TEA)Cl concentration) the relative peak current for **D** declines relative to **D′, C** disappears, and only **B′** is retained (Figure 2(ii,iii,iv)). As **C** is lost, its contribution to the anodic current is transferred to **B′**, i.e. the total **B, B′** + **C** apparently remains constant.

The currents for **D** and **D′** are each linearly dependent upon $v^{1/2}$, with both waves shifting about 20 mV negatively per 10-fold increase of scan rate. In another experiment when 0.15 M TBAP was added to a solution containing 0.05 M (TEA)Cl, there was no apparent change in any of the peak currents. Note also that the relative ratio of currents of **D/D′** is greater in the steady state, Figure 2(iii,iv), than in the first scan Figure 2(ii).

(1.1.3) Ethanol/Dry Ice Bath Temperature (−72 °C). (1.1.3.1) TBAP Electrolyte. Figure 3(ii) shows the CV of species **1,Cl** (DMF, 0.15 M TBAP) solution at −72 °C, compared with the room temperature data in Figure 3(i). Under the low temperature conditions, switching positive of **E**, **D** becomes more reversible, **B′** is weakly observed, and **C** is missing. When scanning negative of couple **E**, much of the anodic current of **D** is again lost, **B′** recovers some additional anodic current and a new cathodic feature, just positive of **E**, labeled **E′** is observable; wave **C** remains absent. If the low temperature solution is allowed to warm up slowly, with continuous scanning from 0 to −1.5 V (positive of **E**), the more reversible **B** grows in as the temperature rises, but **C** does not appear until close to room temperature. This suggests that the species at **B** (not **B′**) and **C** arise from following chemical processes which are inhibited at lower temperature.

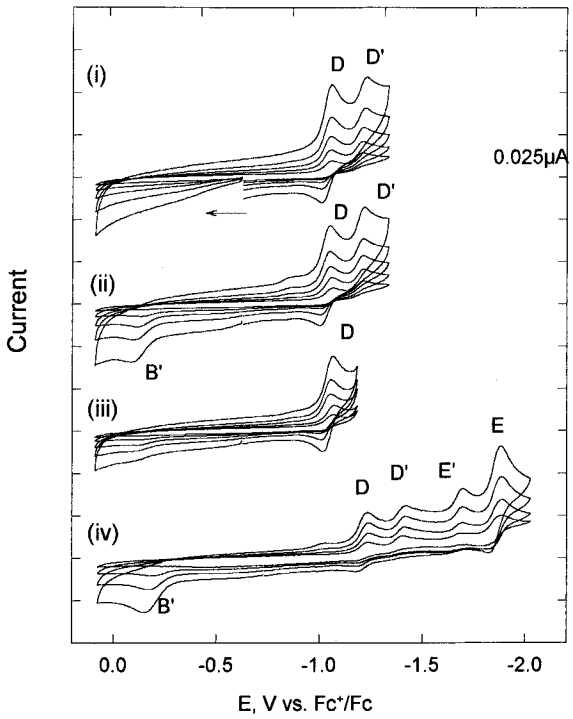

Figure 4. Cyclic voltammogram of ClRh^{III}Pc(2−), (**1,Cl**) in DMF, low temperature, (−72 °C), 0.05 M (TEA)Cl: (i) initial scan, 10, 25, 50, 100, and 200 mV/s; (ii,iii) steady state scan, 10, 25, 50, 100, and 200 mV/s; (iv) steady state scan; 10, 25, 50, and 100 mV/s.

(1.1.3.2) (TEA)Cl Electrolyte (0.05 M). In the first scan (Figure 4(i)) both **D** and **D′** are observed, with **D$_{an}$** being quite prominent; i.e. process **D** approaches reversibility. However **D′$_{an}$** is not observed, **D′** remaining irreversible. If switching occurs between **D** and **D′**, then **D** remains reversible (Figure 4(iii)). In the steady state, switching between **D** and **D′**, no wave is seen at **B′**, but switching negative of **D′** reveals irreversible wave **B′** (Figure 4(ii)). If the CV is switched negative of **E**, then, importantly, **D** becomes largely irreversible again, and wave **B′** grows in relative intensity. Further, the extra wave **E′** is clearly observed.

Note that the ratio **D$_{an}$/D$_{cat}$** is less than one and decreases with decreasing scan rate, viz: **D$_{an}$/D$_{cat}$** = 0.7 at 500 mV/s and 0.3 at 50 mV/s (switching between **D** and **D′**, first scan). At 5 mV/s, **D$_{an}$** is barely perceptible. In the equilibrium scan, wave **B′** also begins to grow at slower scan rates even when switching is between **D** and **D′**. Thus even at −72 °C, the species at **D** dimerizes slowly to form the dinuclear Rh^{II} species, while the species at **D′** rapidly dimerizes at −72 °C.

(1.2) ClRh^{III}TNPc(2−), (TN,1,Cl), at room temperature. The first reduction of (**TN,1,Cl**), wave **D**, in solution (DMF, TBAP, or (TBA)PF$_6$) is about 200 mV more negative than with species **1,Cl** (Figure 5; Table 1) and, unlike the behavior of species **1,Cl**, this redox process appears to be reversible, at fairly high scan rates, if the switching limit is more positive than

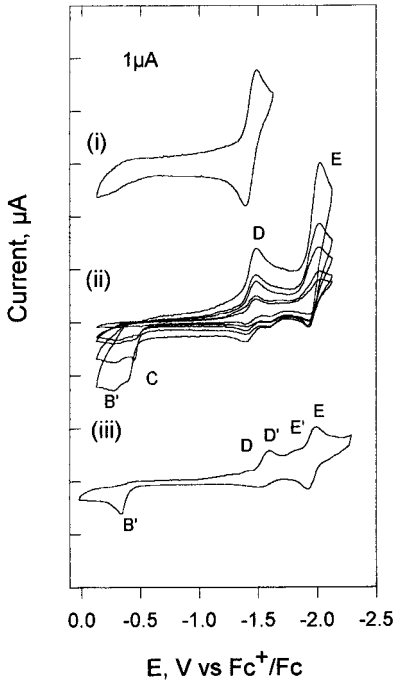

Figure 5. Cyclic voltammograms for species (**TN,1**) in DMF (0.15 M TBAP, Pt working electrode): (i) scan rate 500 mV/s; (ii) scan rate: 25, 50, 100, 200, and 500 mV/s. (iii) Cyclic voltammogram for species (**TN,1**) in DMF (0.15 M (TEA)Cl, Pt working electrode), steady state, scan rate 100 mV/s.

couple **E** (Figure 5(i)). Waves **B, B′,** and **C** are also absent under these conditions. However, at slow scan rate (25 mV/s), $\mathbf{D_{an}}$ becomes significantly less than $\mathbf{D_{cat}}$. Scanning more negative than couple **E** also resulted in a marked reduction in the anodic current for wave **D**, even at higher scan rates and the reappearance of **B, B′**, and **C** (Figure 5(ii)).

With (TEA)Cl (0.15 M) as the supporting electrolyte (Figure 5(iii)), couple **D′** appears as a fairly reversible wave at about 90 mV negative of the position of wave **D** (similar to Figure 5(i), data not shown). Wave **D** however, is essentially absent in the steady state data switched just negative of **D′**; Wave **B′** is weakly observed. Scanning negative of couple **E** resulted in an increase of the current for wave **B′**, couple **D′** becomes irreversible, and the cathodic components of **D** and **E′** are weakly seen (Figure 5(iii)). Waves **B** and **C** are not observed.

(1.3) Dinuclear Rh^{II} Species (3) (Figure 6). Reduction of $ClRh^{III}Pc(2-)$ at wave **D** leads to formation of $[ClRh^{II}Pc(2-)]^-$ (**2,Cl**) which dimerizes at room temperature.[11,12,27] Controlled-potential reduction of species (**1,Cl**), 100 mV negative of wave **D**, then gives rise to a dinuclear species which is generically called the dinuclear Rh^{II} species (**3**) without, for the moment, indicating what the axial ligands are. Here we describe the cyclic voltammetry of this dinuclear species. Note that **TN,1,Cl** similarly gives the dinuclear species under controlled potential reduction negative of **D**, indicating that the steric bulk of the neopentoxy groups while slowing down the dimerization process does not stop it.

The first CV scan, −1.0 to −1.7 V, in species (**3**) bulk solution (DCB or DMF, 0.15 M TBAP) did not show any appearance of wave **D** corroborating that the bulk solution contained only the dinuclear $Rh^{II}Pc$ species (**3**) (Figure 6(i), dotted line). Wave **E** is observed with an $E_{1/2}$ value essentially identical to that of **E** in the CV of species (**1,Cl**), and wave **E′** is not observed (Figure 6(iv,v)). Waves **B, B′**, and **C** are observed, providing proof that these processes involve the dinuclear species (Figure 6).

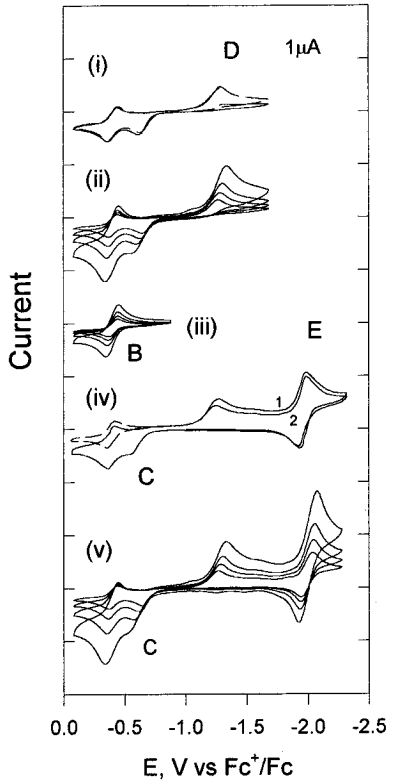

Figure 6. Cyclic voltammograms for dinuclear Rh^{II} species (**3,Cl**) in DCB (0.15 M TBAP, Pt working electrode): (i) scan rate 100 mV/s, initial scan (dot line, negative going from −1.3 V) and steady scan (solid line); (ii) steady state, scan rate 50, 100, 200, and 500 mV/s; (iii) steady state, scan rate 50, 100, 200, and 500 mV/s cycling around **B** only. (iv) After cycling around **B** several times to yield a reversible couple at **B** (hatched line), the negative limit is switched negative of **E**: (1) first scan; (2) second scan; scan rate 100 mV/s. The current scale in this specific experiment is 0.5 μA/division. (v) Voltammograms as in part ii, scanning over a wider range.

Steady state microelectrode analysis in DCB shows waves **B, B′**, and **E** only (not **C**) with equal currents (**B** + **B′** = **E**). Wave **C** is seen in the steady state microelectrode study in DMF, with the combined current **B**, **B′** + **C** = **E**. When one is scanning positive of wave **C** and returning negatively, wave **D** reappears, but with a smaller current, indicating that a Rh^{III} monomer species is recovered positive of **C** (or **B**, **B′**) (Figure 6(i), second scan). Scanning around waves **B**, **B′** and **C**, in DCB, (within the range 0 to −0.8 V) causes the rapid disappearance of wave **C**, within about four scans (100 mV/s, in DCB) until a well-defined reversible redox couple, **B**, ($i_p \propto v^{1/2}$, $i_p^a = i_p^c$, $E_p^a - E_p^b = 70$ mV) was observed (Figure 6(iii)). Note that, in DMF solution, wave **C** is retained under these scanning conditions. Although the anodic wing of **B, B′** appears to decline, in the DCB experiment, it is built upon the positive potential tail of **C** and it seems that the current of **B** remains constant (compare Figure 6 (ii,iii)); note that $\mathbf{B_{cat}}$ is essentially constant in all scans at a given scan rate. Figure 6(iv) shows an experiment where following a scan such as shown in Figure 6(ii), the negative switching potential is changed to about −0.8 V (generating a reversible **B** as shown in Figure 6(iii)) and then, once this is established (Figure 6(iv) dotted line), the negative switching potential is changed to scan out beyond **E**. Significant current is seen at **D** on the *first* negative bound scan showing that mononuclear $Rh^{III}Pc$ species are found at the electrode surface. Waves **B′, C** are recovered when returning positive.

Scanning between 0 and −1.5 V, the ratio of currents **C**/**B** declines with increasing scan rate (Figure 6(ii,v)) as previously noted for the bulk **1,Cl** experiments. Waves **C** and **D** are

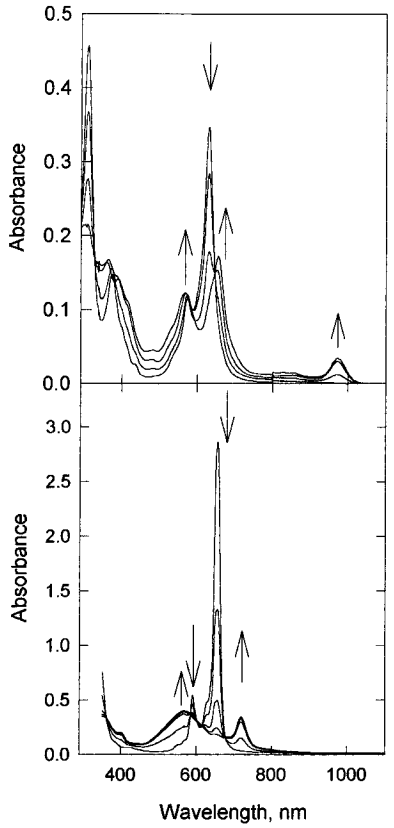

Figure 7. Bottom: Spectroscopic changes during the step-potential for the first oxidation of species (**1,Cl**) in DCB (0.15 M TBAP). Top: Spectroscopic changes during the step-potential for second reduction of species (**1,Cl**), in DMF (0.2 M TBAP) to form **5**.

evidently coupled since wave **C** is lost when scanning around **B, B′**, and **C** unless the negative scan is moved close to that where **D** appears, in which case **C** reappears. Further evidence for coupling is adduced from the faster scan rate studies, over **B, B′**, **C**, and **D**, when as the relative current at **C** declines, so does that at **D**. Note however that while **D** is not observed in the first negative going scan of a freshly stirred dinuclear bulk **3** solution, wave **C** is observed in the first positive going scan toward **B, B′,** and **C**. The anodic current for waves **B** and **C**, lost after the scan shown in Figure 6(iii), can easily be recovered by stirring the solution or scanning to the vicinity of wave **D**. Controlled-potential oxidation of the dinuclear Rh^{II} species (**3**) solution, just positive of wave **B, B′**, yields only a monomeric $PcRh^{III}$ species; on this time scale, the purported dinuclear $PcRh^{III}$ species is unstable.

If chloride ion is added to this dinuclear Rh^{II} solution (**3**), wave **C** loses current with increase of the concentration of chloride ion eventually disappearing. The anodic current of **B, B′** increases, while the cathodic current diminishes and is lost at 0.15 M (TEA)Cl leaving only the anodic wing, of **B′**, appearing as in Figure 2(iii). During this process, the total anodic current remains constant, i.e. the contribution from **C** is transferred to **B′**.

(2) Spectro-electrochemistry (Figures 7 and 8). (2.1) Oxidation. The uv/vis spectroscopic changes during the stepwise oxidation of species (**1,Cl**) in DCB (wave **A**) are shown in Figure 7(bottom). There is growth of a new band at 714 nm, decrease of the intensity of the Q band and its vibrational satellite, and growth of a new feature lying between the Q band and Soret bands. Table 2 summarizes the spectroelectrochemical data. The final spectrum after oxidation just positive of wave **A** is very similar to that of the $Rh^{III}Pc(1-)$ cation radical as reported by Ferraudi,[22] Nyokong,[12a] and also Liu.[12b]

Table 2. Absorption Spectra of Species **1**, **3**, and **4**[a]

species/solvent	wavelength (λ, nm (log ϵ))			
(**1,Cl**)/DMF	346 (4.42)	587 (4.30)	650 (5.05)	
(**1,Cl**)/DCB[b]	349 (4.48)	594 (4.43)	657 (5.21)	
(**TN,1,Cl**)/DMF[c]	347 (4.63)	590 (4.55)	655 (5.24)	
(**TN,1,Cl**)/DCB[c]	342 (4.45)	600 (4.46)	665 (5.15)	
(**TN,1,Cl$_2$**)/DCB[d]	365 (4.46)	595 (4.48)	659 (5.2)	
(**3**)/DMF[b]	308 (4.80)	372 (4.31)	573 (4.20)	629 (4.68)
(**3**)/DCB[c]		372 (4.68)	578 (4.34)	633 (4.80)
(**TN,3**)/DMF[b]	309 (5.02)	367 (4.54)	577 (4.46)	633 (4.86)
(**4,Cl**)/DCB[c]	569 (4.34)	719 (4.27)		
(**TN,4,Cl**)/DMF[b,e]	595	661	714	

[a] Species **3** (dinuclear rhodium(II)) and **4** (Pc(1−) radicals of rhodium(III)) were obtained in a spectroelectrochemical cell by reduction or oxidation of the corresponding species **1**, respectively.[b] 0.15 M TBAP. [c] 0.2 M TBAP. [d] See caption to Figure 8. [e] Incomplete oxidation.

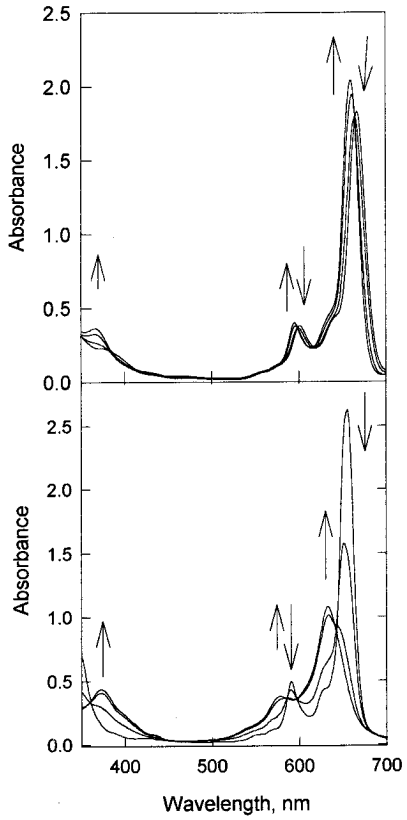

Figure 8. Bottom: Spectroscopic changes during the step-potential for the first reduction for species (**1,Cl**) in DCB (0.15 M TBAP) to form **3**. Top: Spectroscopic changes observed during the addition of (TEA)Cl to a solution of $ClRh^{III}TNPc$ (**TN,1,Cl**) in DCB, forming **TN,1,Cl2**: top spectrum, pure (**TN,1,Cl**); subsequent spectra have molar ratios of Cl:(**TN,1,Cl**) of 0.45, 0.9, 4.5, and 22.5, respectively.

(2.2) Reduction between Waves D and E. Figure 8(bottom) shows the UV/vis spectroscopic changes for a DCB solution of species **1,Cl** during the stepwise reduction just negative of the first reduction wave **D**. The Q band broadens, weakens in molar intensity, and shifts to the blue, but no additional absorption is noted either to longer wavelengths of the Q band or in the region between the Q and Soret bands (Table 2). The absence of such bands illustrates that the phthalocyanine ring is neither reduced nor oxidized.[34] The shift in Q band is consistent with formation of a dinuclear MPc species, presumably $[XRh^{II}Pc(2-)]_2$, (**3**), where we comment later on the nature of X. A metal-based

(34) Stillman, M. J. In *Phthalocyanines: Properties and Applications*; Leznoff, C. C., Lever, A. B. P., Eds.; VCH: New York, 1993; Vol. 3, p 227.

reduction forming a dinuclear species was also confirmed by Nyokong.[12a] Our spectrum of the dinuclear species agrees with data reported by Liu (Figure 4[12b]) and also Nyokong (Figure 4[12a]) except that the latter shows a peak at ca 650 nm which is clearly due to contamination by unreduced starting material (monomeric Rh(III)Pc); no such peak is present in our spectrum (Figure 8(bottom)).

(2.2.1) Oxidation Positive of Waves B, C. Since the dinuclear (**3**) voltammogram exhibits a reversible wave **B**, an attempt was made to obtain the electronic spectrum of the presumed dinuclear Rh^{III} species. However it is insufficiently stable under the controlled-potential time scale, and only a monomeric $Rh^{III}Pc(2-)$ species is obtained.

(2.3) Reduction Negative of Wave E. Figure 7(top) shows the UV/vis spectroscopic changes for a DMF solution of species **1,Cl** during the stepwise reduction just negative of wave **E**. New bands arise at 654 and 567 nm and at 973 and 832 nm in the near-IR region. The spectrum is fully consistent with formation of an anion radical, Pc(3−) species.[34] In DCB solution, decomposition of the anion radical was observed with loss of isobestic points before completion of the reduction; this also precluded obtaining a reliable cyclic voltammogram of this bulk species.

(3) Spectroscopy of Rhodium(III) Phthalocyanines. The appearance of wave **D′** on addition of excess chloride ion is most readily associated with the formation of an additional chloro species in solution. Thus the electronic spectrum of $ClRh^{III}TNPc(2-)$, (**TN,1,Cl**), in DCB was compared with that in the presence of excess chloride ion. Figure 8(top) shows that there are indeed distinct changes in the electronic spectrum consistent with formation of a new species, presumably $[Cl_2Rh^{III}TNPc(2-)]^-$ (**TN,1,Cl$_2$**). These effects are observable even at a 1:1 ratio of $ClRh^{III}TNPc(2-)$:Cl showing a high binding constant for chloride ion. Similar effects are observed with the unsubstituted **1,Cl** except that higher concentrations of chloride ion are needed; i.e. the binding constant is smaller.

Discussion

(1) Rhodium(III) Species in Solution. In the discussion which follows it may be assumed that the species **1,Cl** and **TN,1,Cl** behave in a parallel fashion unless differences are specifically mentioned. Since $ClRh^{III}Pc(2-)$ (**1,Cl**) is soluble in the noncoordinating solvent DCB and has a spectrum therein very similar to that in DMF, it is reasonable to assume that the species in these solutions is the five coordinate moiety. In DMF, weak binding to the solvent forming a six coordinate species cannot be excluded but does not alter the overall conclusions (compare data in Figures 1 and 3). The addition of excess chloride ion results in some small changes in the electronic spectrum (Figure 8(top)) and profound changes in the cyclic voltammogram (appearance of wave **D′**), most easily interpreted by the equilibrium

$$ClRh^{III}Pc(2-)\ (\mathbf{1,Cl}) + Cl^- \rightleftharpoons [Cl_2Rh^{III}Pc(2-)]^-\ (\mathbf{1,Cl_2}) \quad (1)$$

Equilibrium 2 must also be considered:

$$ClRh^{III}Pc(2-) + ClO_4^- \rightleftharpoons (ClO_4)Rh^{III}Pc(2-)] + Cl^- \quad (2)$$

Adding excess TBAP (0.15 M) to a solution containing a low concentration of (TEA)Cl (0.05 M) led to no change in the cyclic voltammogram, specifically no change in the relative magnitudes of the currents of any of the waves; thus equilibrium 2 is deemed unimportant. Equilibrium 1 must be very slow to reverse since otherwise the cyclic voltammogram would only exhibit wave **D** with species **1,Cl$_2$** undergoing a CE reaction[35] at **D**, the "C" being the reverse of (1); this is not observed. Indeed both the forward and return rates for equilibrium 1 must be slow since the **D**/**D′** current ratio is so much greater in steady state scans than in the initial scan (Figure 2(ii,iii) and data in Figure S1) indicating that **1,Cl** is formed upon oxidation at **B′,C** and does not readily convert to **1,Cl$_2$** on the time scale of the faster scans.

Species **1,Cl$_2$** is some 200 mV more difficult to reduce to **2,Cl$_2$** than **1,Cl** and similarly is 90 mV more difficult for **TN,1,-Cl$_2$** (Table 1). The negative shift in potential is consistent with the additional negative charge on these six coordinate species. The shift of 200 mV for species **1,Cl** conversion to **1,Cl$_2$** cannot be reliably converted into a binding constant for the second chloride ion since the observed reduction waves are irreversible.

(1.1) Oxidation of Chlororhodium(III) Phthalocyanine species. The oxidation side is quite straightforward with both **1,Cl** and **TN,1,Cl** being oxidized, at wave **A**, to the cation radical, $[ClRh^{III}Pc(1-)]^+$ (**4**) as proven by spectroelectrochemistry (Table 2). Its photochemical behavior has previously been studied by Ferraudi and co-workers.[20,22,26] The oxidation is reversible but the species was not further investigated. The steady state microelectrode study shows that waves **A**, **D**, and **E** all have essentially the same steady state current (Figure 1(ii)); since **A** unequivocally involves the $1e^-$/Rh oxidation of (**1,Cl**) then **D** and **E** are defined each one as $1e^-$/Rh or equivalently $2e^-/Rh_2$ dinuclear processes.

(1.2) Reduction of Chlororhodium(III) Phthalocyanine Species. To summarize the results which will be proven below, $ClRh^{III}Pc(2-)$ (**1,Cl**) undergoes a one-electron reduction to $[ClRh^{II}Pc(2-)]^-$ (**2,Cl**), which rapidly dimerizes, at room temperature, initially forming six-coordinate $[Pc(2-)(Cl)Rh^{II}\text{-}Rh^{II}(Cl)Pc(2-)]^{2-}$ (**3,Cl$_2$**), with a rhodium−rhodium bond, such that the reduction process (wave **D**) is electrochemically irreversible. The dinuclear species **3** may be further reduced (wave **E**, reversible) to form the $[Rh^{II}Pc(3-)]_2$ dinuclear anion radical species **5**. Two-electron re-oxidation of the dinuclear Rh^{II} species **3** would yield a dinuclear Rh^{III} species (**6**), which would dissociate back to monomeric rhodium^{III} species rapidly or slowly depending on the nature of the axial ligand (waves **B**, **B′**, and **C**).

Alternatively, the dinuclear Rh^{II} species may undergo, in the region of **B, B′,** and **C** a one-electron oxidation to a mixed-valence species, $Rh^{II}Rh^{III}$ which then dissociates rapidly to a Rh^{II} and a Rh^{III} species, with the former then oxidizing to Rh^{III} since it will be sitting at the electrode polarized at a potential more positive than the mononuclear $Rh^{III} \rightarrow Rh^{II}$ process (wave **D**). This would be an ECE process, while the two-electron oxidation would be an EEC process.[35] It is not possible, from the data available, to distinguish between these two processes. However reversible wave **B** is definitely a two-electron oxidation, on the basis of the steady state data, and we will suppose that oxidation at **B′** and **C** are also two-electron processes, EEC. If they should actually be ECE processes, it makes very little difference to the overall analysis. As we will demonstrate, the data are consistent with the existence of three different dinuclear Rh^{II} species, namely $[Pc(2-)(Cl)Rh^{II}.Rh^{II}(Cl)(Pc(2-)]^{2-}$ (**3,Cl$_2$**), $[Pc(2-)(Cl)Rh^{II}Rh^{II}Pc(2-)]^-$ (**3,Cl**), and $[Pc(2-)Rh^{II}Rh^{II}Pc\text{-}(2-)]$ (**3,none**) (this last may have a weakly coordinated ClO_4^-

(35) Bard, A. J.; Faulkner, L. R. *Electrochemical Methods; Fundamentals and Applications*; John Wiley and Sons: New York, 1980. CE is electrochemical notation for a reversible chemical reaction preceeding a reversible electron transfer process.

ion). Oxidation of these three species gives rise to waves **B′**, **C**, and **B** respectively. The process at **B** is reversible showing that a dinuclear $Rh^{III}Pc$ species (**6**) survives on the electrochemical time scale and is observed to be irreversibly oxidized at **A′**. One may also presume the presence of the three correspondingly coordinated $[Rh^{II}Pc(3-)]_2$ species labeled **5,Cl$_2$**, **5,Cl**, and **5,-none**. At −72 °C using **1,Cl**, or starting from **TN,1,Cl** at room temperature, dimerization is inhibited (reversible wave **D**) and mononuclear $[ClRh^{II}Pc(2-)]^-$ species (**2,Cl**) can be observed.

In the presence of excess chloride ion, the chemistry is similar but begins with reduction of the six coordinate (**1,Cl$_2$**) to an anion radical of Rh^{III}, namely $[Cl_2Rh^{III}Pc(3-)]^{2-}$ (**7,Cl$_2$**) which subsequently loses chloride and dimerizes forming, initially, (**3,-Cl$_2$**).

The complex equilibria generated upon reduction of species **1** are summarized in Scheme 1. We now discuss how the various redox processes and equilibria in Scheme 1 can be confirmed by appropriate analysis of the Results described above.

(1.2.1) Dimerization Largely Inhibited. At low temperature (−72 °C), (**1,Cl**) can be reduced near −1.2 V (DMF, TBAP, wave **D**) in a process which is almost reversible provided that the sweep is switched positive of **E** (Figure 3(ii)). However, $ia < i_c$ for wave **D**, indicating that even under these conditions some dimerization occurs and is evident in the appearance of a small anodic current for **B′**. Essentially the same behavior may be observed on the cyclic voltammogram time scale, at room temperature, using the sterically more crowded $ClRh^{III}TNPc(2-)$ (**TN,1,Cl**) (Figure 5). However on the controlled-potential reduction time scale, reduction of **TN,1,Cl** at room temperature, just negative of wave **D**, leads to formation of the dinuclear species **TN,3**. Note that in both the low temperature experiment (Figure 3(ii)) and the experiment with **TN,1,Cl**, if cycling is continued negative of wave **E**, then **D$_{an}$** is largely lost and **B, B′**, and **C** are more prominent. Thus cycling beyond **E** facilitates the dimerization process.

The mononuclear Rh^{II} species is susceptible to dimerization even at low temperatures; thus its characterization is difficult. Since the dinuclear **3** clearly contains $Rh^{II}Pc(2-)$ (cf. electronic spectra, Figure 8(bottom)), it is reasonable to suppose that the mononuclear species, **2**, does indeed contain the $Rh^{II}Pc(2-)$ unit. It is convenient to discuss each region of the cyclic voltammogram in turn, beginning with the gross features of the voltammetry.

(1.3) Wave D (Figure 1). Controlled potential electrolysis of **1,Cl** just negative of wave **D**, at room temperature, provides the dinuclear species **3** as previously commented.

$$\underset{\textbf{1,Cl}}{ClRh^{III}Pc(2-)} + e^- \rightarrow \underset{\textbf{2,Cl}}{[ClRh^{II}Pc(2-)]^-} \quad (3)$$

$$\underset{\textbf{2,Cl}}{2[ClRh^{II}Pc(2-)]^-} \rightarrow \underset{\textbf{3,Cl}_2}{[ClRh^{II}Pc(2-)]_2^{2-}} \quad (4)$$

The dimerization process is proven by the electronic spectrum of the product (Figure 8(bottom)), the concentration dependence study of the potential of **D**, and the scan rate dependence which is that expected for such an irreversible process.[35] Given the natural proclivity of Rh^{II} to dimerize via formation of a Rh−Rh bond, this result is unsurprising and similar to the behavior of rhodium porphyrins.[31,36,37] The current on wave **D** on the second scan is always appreciably less than the first scan (Figure 1(iv)) but reaches equilibrium in later scans. This observation is explained by depletion of the bulk species **1,Cl** at the electrode surface because the dinuclear Rh^{II} species that is formed oxidizes to a Rh^{III} dinuclear species (at **B**) which has some stability on the electrochemical time scale (partially reversible) (*vide infra*) and only a fraction of this dissociates back to **1,Cl** by the time the sweep returns to **D**.

(1.3.1) Wave D′ (Figures 2, 4, and 5). This irreversible wave is observed in the presence of (TEA)Cl, when species **1,Cl$_2$** is present and is therefore a reduction product of **1,Cl$_2$**. The reduction product cannot be $[Cl_2Rh^{II}Pc(2-)]^{2-}$ since this species must surely lose chloride ion first (it has a d_{z^2} configuration) to generate species **2,Cl** which would then dimerize to **3,Cl$_2$**. However at −72 °C, reduction at **D′** is irreversible, forming the dinuclear species (appearance of wave **B′**, Figure 4), yet under these conditions **2,Cl** does not dimerize (wave **D** is reversible). Further, if **D′** is assigned to formation of $[Cl_2Rh^{II}Pc(2-)]^{2-}$, the irreversibility of this couple is surely then explained by loss of chloride ion; if this occurs, the wave **D$_{an}$**, which represents oxidation of this latter species, would be larger when switching negative of **D′** than negative of **D**. This is certainly not the case. There will be a slight loss in current at **D$_{an}$** when scanning negative of **D′** relative to scanning negative of **D** (due to the extra time allowed for the slow dimerization) but this is certainly not sufficient to offset the growth in **D$_{an}$** which would occur if $[ClRh^{II}Pc(2-)]^-$ were a product generated at **D′**. This argument is especially cogent at higher scan rates. Thus the species at **D′** *cannot dimerize via a pathway proceeding via the species at **D***.

Whether or not reduction occurs at the metal center or the phthalocyanine ring depends generally on the relative energies of the metal d_{z^2} orbital and the Pc π^* orbital (though subsequent relaxation means this argument should be treated cautiously). The six coordinate $L_2Rh^{III}Pc(2-)$ will necessarily have a significantly higher d_{z^2} energy than the five-coordinate $LRh^{III}Pc(2-)$, and Nyokong[12a] has argued convincingly that when L = CN^-, reduction occurs at the phthalocyanine ring. On the basis of electrochemical parameter relationships[38−41] the $L_2Rh^{III}Pc(2-)/L_2Rh^{II}Pc(2-)$ couple for L = Cl^- must be significantly negative of that of L = CN^-. Thus if phthalocyanine ring reduction occurs for L = CN^-, it should certainly also do so for L = Cl^- in the $L_2Rh^{III}Pc(2-)$ species.

If reduction first occurs at the ring and then this anion radical loses a chloride atom and dimerizes, this provides an alternate pathway which need not, and presumably does not, proceed through **2,Cl** providing an explanation for the difference in behavior at **D** and **D′** in the low temperature data (Figure 4).

$$\underset{\textbf{1,Cl}_2}{[Cl_2Rh^{III}Pc(2-)]^{2-}} + e^- \rightarrow \underset{\textbf{7,Cl}_2}{[Cl_2Rh^{III}Pc(3-)]^{3-}} \quad (5)$$

$$\underset{\textbf{7,Cl}_2}{2[Cl_2Rh^{III}Pc(3-)]^{3-}} \rightarrow \underset{\textbf{3,Cl}_2}{[ClRh^{II}Pc(2-)]_2^{2-}} + 2Cl^- \quad (6)$$

Returning to the aforesaid slow rate of conversion of **1,Cl** to **1,Cl$_2$** and vice versa, the steady state concentration of **1,Cl** at the electrode is proportionately larger than in the bulk, as illustrated by comparison of the first scan with the steady state

(36) Felthouse, T. R. *Prog. Inorg. Chem.* **1982**, *29*, 73.
(37) Lee, S.; Mediati, M.; Wayland, B. *J. Chem. Soc., Chem. Commun.* **1994**, 2299. Boyar, E. B.; Robinson, S. D. *Coord. Chem. Rev.* **1983**, *50*, 109.
(38) Lever, A. B. P. *Inorg. Chem.* **1990**, *29*, 1271.
(39) Lever, A. B. P. *Inorg. Chem.* **1991**, *30*, 1980.
(40) Lever, A. B. P. In *Proceedings of the NATO Advanced Workshop-Molecular Electrochemistry of Inorganic, Bioinorganic and Organometallic Compounds*; Pombeiro, A. J. L., McCleverty, J. A., Eds.; Kluwer Academic Publishers: Sintra, Portugal, 1992; p 41.
(41) Masui, H.; Lever, A. B. P. *Inorg. Chem.* **1993**, *32*, 2199.

scan; compare the ratio of **D**/**D′** in Figure 2(ii,iii). This is explained by the generation of **1,Cl**, rather than **1,Cl$_2$**, upon oxidation at **B′**. In fast scans there is no time to requilibrate to **1,Cl$_2$**, and so **D** is proportionately larger. In slow scans, there is such time for equilibration and **D** is relatively much less prominent. Note that the spectroscopic data show that **TN,1,-Cl$_2$** is a more stable species than **1,Cl$_2$** and this is reflected in the electrochemistry described in section 1.2.1 in the Results where wave **D** is absent in the steady state CV scan (Figure 5(iii)).

(1.4) Wave E (Figures 1−6). The subsequent reduction, wave **E**, is reversible and corresponds to

$$\underset{\textbf{3,Cl}_2}{[\mathrm{ClRh^{II}Pc}(2-)]_2^{2-}} + 2e^- \rightarrow \underset{\textbf{5,Cl}_2}{[\mathrm{ClRh^{II}Pc}(3-)]_2^{4-}} \quad (7)$$

Controlled potential reduction just negative of wave **E** yields a solution with the electronic spectrum shown in Figure 7(top) consistent with a radical anion Pc(3−) species. However this solution is not very stable, and the possibility that a Rh^{I} species is formed is not excluded by the electronic spectrum. On the basis of comparative behavior with CoPc chemistry, a [Rh^{I}Pc-(2−)]$^-$ species is unlikely. The reduction process **E** follows the Rh^{III}Pc(2−)/Rh^{II}Pc(2−) couple, **D** by some 500 mV. Indeed since the process at **D** is irreversible, the true thermodynamic difference between these processes is less than 500 mV. The Co^{II}Pc(2−)/Co^{I}Pc(2−) process is some 700−1000 mV more negative than Co^{III}Pc(2−)/Co^{II}Pc(2−) depending on the substituent.[1] Similarly the Fe^{III}Pc(2−)/Fe^{II}Pc(2−) process is separated from Fe^{II}Pc(2−)/Fe^{I}Pc(2−) by about 1000 mV. These data argue for ring rather than rhodium ion reduction, though the cobalt and rhodium systems are sufficiently different that arguments about rhodium based upon cobalt should be interpreted with care. More persuasive is the argument that the species formed at **E** is dinuclear. When **TN,1,Cl** is reduced at room temperature and switched between **D** and **E**, the return wave **D$_{an}$** is observed, and wave **B** is weak, showing that dimerization is inhibited. If switching occurs negative of **E**, then **D$_{an}$** is absent and **B** is relatively stronger (Figure 5). Similarly in the low temperature experiments in Figure 3(ii), and in Figure 4, wave **D$_{an}$** (oxidation of mononuclear **2**), is proportionately weaker when switching is negative of **E**. Therefore the species at **E** must favor dimerization, i.e. the mononuclear (**TN,2,Cl**) must dimerize following reduction at **E**.

It is certainly reasonable that the species [ClRh^{II}Pc(3−)]$^{2-}$ (**8,Cl**) would dimerize more readily than [ClRh^{II}Pc(2−)]$^-$ (**2,-Cl**) because of the additional negative charge rendering the Rh^{II} d_{z^2} orbital more diffuse. One may conclude from these data that a dinuclear species, such as **3** will remain dinuclear upon reduction at **E**, and further that these species do indeed contain Rh^{II}Pc(3−) (d^7) and not Rh^{I}Pc(2−) (d^8) since the latter species would show no tendency to dimerize.

(1.4.1) Wave E′ (Figures 3−5). A small additional wave, just positive of **E**, and labeled **E′**, is frequently seen when dimerization is inhibited, either by use of the TN species or in the low temperature studies. Since this is only observed when the mononuclear [ClRh^{II}Pc(2−)]$^-$ (**2,Cl**) species is present at the electrode, process **E′** is most readily ascribed to reduction of this species to mononuclear [ClRh^{II}Pc(3−)]$^{2-}$ (**8,Cl**) which must then rapidly dimerize (no return wave). That **2,Cl** would be reduced at a more positive potential than **3,Cl** is consistent with the extra negative charge on the latter species.

(1.5) Voltammetry of the Dinuclear Species 3 (Figure 6). The bulk dinuclear species **3** has no reduction wave at **D** on the first negative going scan from 0 V, but does furnish **B**, **B′**, and **C** on the first scan, confirming that these processes are indeed located on the dinuclear species. On the second, and subsequent scans, switching positive of **B** or **C**, wave **D** is observed since "new" monomeric species are generated at the electrode surface, following oxidation at **B′** and **C** (Figure 6-(i,ii,iv,v)). The steady state data reveal that the combined currents for **B**, **B′**, and **C** correspond with 2e$^-$ per dinuclear molecule.

(1.6) Nature of B, B′, and C. One of the more interesting and perplexing aspects of the electrochemistry of species **1,Cl** is the specific identities of the processes generating waves **B**, **B′**, and **C** involving the dinuclear species **3** and an explanation of their complex behavior. It is necessary to explain the following special characteristics of the **B**, **B′**, and **C** set of waves.

(i) Wave **C** is absent from low temperature studies (Figure 3(ii)).

(ii) The current ratio **C**/**B** reduces with increasing scan rate (Figure 1 (v), Figure 6 (ii,v)).

(iii) The shift to more positive potential for wave **C** that occurs with increasing scan rate and its simultaneous loss of current while the total current **B**, **B′** + **C** remains constant (and **D** also diminishes in the bulk dinuclear system).

(iv) The loss of **B** and **C** that takes place in the presence of chloride ion, leaving only irreversible **B′**. Indeed the appearance of only **B′** in the low temperature voltammogram and in the room temperature with excess chloride; compare Figures 2, 3(ii), 4, and 5(iii).

(v) The loss of **C** and generation of a reversible wave at **B** that is observed, i.e. loss also of **B′**, when scanning around **B**, **B′**, and **C** in the bulk dinuclear system.

(vi) Following point v, wave **C** reappears if scanning is continued negatively to the vicinity of wave **D**, or if the solution is stirred.

(vii) The steady state microelectrode study of a bulk solution of the dinuclear species **3** in DCB shows no current at **C**, but has total current at **B** equal to that of wave **E** (=2e$^-$/Rh$_2$).

The appearance under various conditions of an irreversible wave at **B′** and at **C** and a reversible wave at **B** argues for three discrete species which have already been suggested to be the three dinuclear Rh^{II} species **3** with 2, 1, or 0 axial chloride ligands respectively. Given the use of the d_{z^2} orbital to bind the two Rh^{II}Pc centers together, the axial linkage to chloride will necessarily be weak and even weaker in the corresponding Rh^{II}Pc(3−) species (beyond **E**); thus, equilibration to form these three species is very reasonable. We now propose a model which, using these three species, will reproduce the properties outlined above.

On the basis of the steady state data, all three species are presumed to oxidize via a 2-electron process (see comments above) to a Rh^{III} dinuclear species which is stable on the electrochemical time scale at **B**, but not at **B′** or **C**. The reappearance of mononuclear Rh^{III}Pc(2−) following oxidation in the **B**, **B′**, and **C** region is confirmed by the appearance of **D** in the voltammetry of the bulk dinuclear species **3** on the second and subsequent scans (Figure 6(i)). The reversible process at **B** must be a two-electron process since its steady state current is equal to that at **E**, and if one were to suppose it were due to a one-electron process to a mixed-valence species, one must expect a second wave corresponding to oxidation of this mixed valence species at some 50−200 mV more positive a value, and this is not observed.

The addition of (TEA)Cl to a solution containing TBAP causes the loss of waves **B** and **C** leaving the irreversible anodic **B′**. The most reasonable explanation is that **B′** corresponds with the irreversible oxidation of the diaxially coordinated Rh^{II}

dinuclear species **3,Cl$_2$**, which should be the dominant species under high chloride ion conditions. Thus at **B′**, **3,Cl$_2$** is fully reoxidized to two molecules of **1,Cl** which is then rereduced at **D** explaining the coupling of **C** with **D**. The presence of chloride ion bound to the Rh^{III}Pc generated would stabilize this species and provide the driving force for decomposition of the initially formed [Pc(Cl)Rh^{III}Rh^{III}(Cl)Pc], **6,Cl$_2$**. The low temperature data, where only **B′** is observed (Figure 3(ii)) reflect the reoxidation of **3,Cl$_2$** which at these low temperatures does not release its axial chloride ions. Reversible wave **B** is then logically assigned to oxidation of **3,none** since the scission to two Rh^{III}Pc species each lacking an axial chloride would be much less facile than the scission of **6,Cl$_2$**. Wave **C** then arises from the half-axially-coordinated (**3,Cl**) which upon two-electron oxidation would yield **1,Cl** plus **1,none**. Thus oxidation of (**3,Cl$_2$**) and (**3,Cl**) is completely irreversible on the CV time scale at room temperature, while **3,none** is reversible (but see caveat below).

To explain the experimental data, in DCB, in some detail, it is necessary to conclude that in the bulk dinuclear solution, the initially formed **3,Cl$_2$** dissociates almost totally to **3,none** at room temperature, viz:

$$\mathbf{3,Cl_2} \rightleftharpoons \mathbf{3,Cl} + Cl^- \rightleftharpoons \mathbf{3,none} + 2Cl^- \qquad (8)$$

Thus the appearance of **C** is a potential driven process whereby as scanning proceeds positively towards **C**, equilibrium 8 drives backward to generate some **3,Cl** for oxidation at **C**. At high scan rates, there is no time for this process to occur, and so wave **C** decreases in relative current and, being irreversible, will shift to more positive potentials. Since **C** does not become the sole wave at the slowest scan rate (1 mV/s) the reequilibration rate for (8) must be slow on the CV time scale. The total current at **B**, **B′**, and **C** represent the total net species **3** present and so equals that at **E** (steady state, bulk **3**). If equilibrium 8 were not almost fully to the right, so that species **3,Cl** and **3,Cl$_2$** were each present to some reasonable amount in the bulk solution, then we would expect that upon cycling around **B**, **B′**, and **C**, the relative currents of **B′** and **C** would diminish but not decline to zero. Simulation (see Supporting Information) reveals that the complete loss of **B′** and **C** can only be explained if they are present in the bulk to a very small extent, i.e. equilibrium 8 lies almost totally to the right. Since Cl^{III}RhPc is ultimately the final product of oxidation at **C** (and at **B′**), then wave **C** must clearly be coupled to wave **D** as observed.

Clearly in this model, **B′** and **C** are recovered if the solution is stirred, after scanning around **B**, **B′**, and **C**, or if scanning proceeds to the region of **D**. The absence of **B** and **C** from low temperature data reflects the sluggishness of (8) at low temperature, and indeed this observation is itself an indicator that process **C** involves a chemical reaction. Thus all the features commented upon above can be explained by this model. In the Supporting Information we show some simulated cyclic voltammograms using this model as a mechanism in the Digisim[42] program. All the features of the experimental observations are reproduced. Because of the large number of species and very considerable number of thermodynamic and kinetic variables involved, a quantitative fit to the experimental data is not attempted. The qualitative fit which can explain all the myriad observations discussed in depth above is itself sufficient proof of the mechanism shown overall in Scheme 1.

We can now also conclude that the spectrum shown in Figure 8, lower, is primarily due to **3,none**. The fact that wave **C** is not totally lost when scanning around the region **B**, **B′**, and **C** of the bulk dinuclear species, in DMF, in contrast to DCB, and appears in the steady state voltammogram, is necessarily explained by assuming that equilibrium 8 lies less completely to the right in DMF.

The cyclic voltammetry of ClRh^{III}Pc adsorbed on highly oriented pyrolytic graphite was reported several years ago.[11] It presented a somewhat simpler picture whose fundamental features are now confirmed by this solution study. The binuclear rhodium(III) species **6** may retain a net Rh^{III}.Rh^{III} bond before reorganization and scission since the HOMO orbital in a Rh^{II}-Rh^{II} fragment is π^* or δ^* in character[43] and loss of electrons therefrom will not initially cause a major change in the RhRh bond strength.

(2) Conclusions. Thus chlororhodium phthalocyanine undergoes a complex series of equilibria upon reduction yielding three species with distinctly different oxidative electrochemistry. Further, the reduction process may be located at the phthalocyanine ring or at the metal center depending upon the nature, if any, of the axial groups. This chemistry has been unraveled by a complex set of optical and electrochemical experiments, at room and low temperatures, and by analysis of data from both the bulk monomeric Rh^{III}Pc species and bulk dinuclear Rh^{II}Pc species, with attention to variable scan rate and microelectrode steady state data, and with simulation using Digisim.

The assignment of the species at **B** and **C** to oxidation of **3,none** and **3,Cl** respectively rests upon our detailed understanding of the behavior of waves **B**, **B′**, and **C** with scan rate and excess chloride ion, upon digital simulation, and upon the expectation that the dinuclear rhodium(III) species **6,none** would have a longer lifetime than **6,Cl**. There is one observation that would argue for the reverse assignment. A frozen solution (Figure 3(ii)) corresponds to 100% generation of **3,Cl$_2$** since the axial chloride is not lost upon reduction of **1,Cl** at wave **D** (equilibrium 8 lies to the far left). Upon warmup, wave **B** grows in before wave **C**; this might then argue for the species at **B** to be **3,Cl** since surely this species will form before **3,none**.

The tetraphenylporphyrin analogs, Cl(L)Rh^{III}TPP and [L$_2$-Rh^{III}TPP]Cl (L = dimethylamine) species studied by Kadish et al.,[29] have cyclic voltammograms which have a gross similarity to the CV of **1** in DCB with respect to the processes at **A**, **D**, and **E**. A dinuclear (TPP)Rh^{II} species is obtained at **D** but unlike the phthalocyanine series, it displays a single irreversible oxidation wave. The detailed chemistry of the L$_2$Rh^{III}TPP series is however very dependent upon the nature of L.[28−31]

The work of Nyokong[12a] shows that the reductive electrochemistry of rhodium(III) phthalocyanine can be modified by changing the axial ligands; thus rhodium phthalocyanine is probably also capable of the very varied electrochemical behaviour already demonstrated by Kadish for the TPP analog.[28−31]

Acknowledgment. The authors are indebted to the Natural Sciences and Engineering Research Council (Ottawa) for financial support, and to Drs. Steven Feldberg and Anton A. Vlcek for assistance with Digisim.

Supporting Information Available: Text giving details of the simulation of some of the cyclic voltammetric data is provided, making use of Digisim (Bioanalytical Systems Inc.), together with a listing of the relevant parameters. Figure S1 shows additional data for species (**1,Cl**) in DMF containing 0.05 M (TEA)Cl. Figures S2−4 contain simulations of waves **B**, **B′**, **C**, **D**, **D′**, and **E** under various conditions (7 pages). Ordering information is given on any current masthead page.

IC950618N

(42) Feldberg, S.; Rudolph, M. Bioanalytical Systems Inc., West Lafayette, IN 47906.

(43) Cotton, F. A.; Wilkinson, G. *Advanced Inorganic Chemistry*, 5th ed.; John Wiley and Sons: New York, 1988; p 1088.